Targeted Masking Enables Stable Cycling of $LiNi_{0.6}Co_{0.2}Mn_{0.2}O_2$ at 4.6 V

Qiao Hu[1], Yufang He[1], Dongsheng Ren[1], Youzhi Song[1], Yanzhou Wu[1], Hongmei Liang[1], Jinhui Gao[1,3], Gang Xu[3], Jiyu Cai[2], Tianyi Li[4], Hong Xu,[1] Li Wang[1*], Zonghai Chen[2*], Xiangming He[1*]

Dr. Qiao Hu, Dr. Yufang He, Dr. Dongsheng Ren, Dr. Youzhi Song, Dr. Yanzhou Wu, Hongmei Liang, Jinhui Gao, Dr. Jiang Zhou, Prof. Dr. Hong Xu, Prof. Dr. Li Wang, Prof. Dr. Xiangming He Institute of Nuclear and New Energy Technology, Tsinghua University, Beijing, 100084, China
E-mail: *wang-l@tsinghua.edu.cn* (L.W.), *hexm@tsinghua.edu.cn* (X. H.)

Dr. Jiyu Cai, Dr. Zonghai Chen
Chemical Sciences and Engineering Division, Argonne National Laboratory, Lemont, IL, 60439, USA
E-mail: *zonghai.chen@anl.gov* (Z. C.)

Dr. Tianyi Li
X-ray Science Division, Advanced Photon Sources, Argonne National Laboratory, 60439, USA

Jinhui Gao, Dr. Gang Xu
Tianjin Lishen Battery Joint-Stock Co., Ltd., Tianjin 300384, China

Keywords: NCM622, parasitic reaction, thermal runaway, high voltage, surface decoration

Abstract

Layered $LiNi_xCo_yMn_{1-x-y}O_2$ (NCM, or NCMxy(1-x-y)) is a dominant family of cathode materials for lithium-ion batteries (LIBs) due to its high energy density. Among all NCM cathode materials, NCM622 possess the optimal energy density at high potential (≥ 4.6 V *vs.* Li/Li^+). However, the practical application of NCM622 at high voltage (≥ 4.6 V) is limited by its parasitic reactions and associated safety concerns. Completely physical isolation has been considered as the main approach to mitigate the parasitic reaction. It has also been previously demonstrated that the interface reaction has active site selectivity, and that the reactivity of the active sites can effectively suppressed by blocking the chemically active sites. Herein, a targeted masking by $LiFePO_4$@C nanoplates is reported to unlock the stable performance of NCM622 up to 4.6 V *vs.* Li/Li^+. The (targeted masked-NCM622)|graphite pouch cell shows

86.5% capacity retention after 1000 cycles and its maximum temperature during thermal runaway is dramatically reduced from 570 °C to 415 °C. Systematic *in/ex* situ characterizations, first-principles calculations and half/pouch cell evaluation prove that PO_4^{3-} is preferentially adsorbed on transition metal sites, stabilizing both the transition metal ions and oxygen ions on the surface against the ethylene carbonate-containing traditional electrolyte even under high voltage (≥ 4.6 V *vs.* Li/Li^+). This work opens up new venue for rational design of high-performance cathode materials through a low-cost and scalable decoration process, and reveal a new understanding of interfacial activity of materials.

1. Introduction

The ever-increasing energy consumption of modern society demands energy storage technology with increasing energy density.[1-3] Lithium-ion batteries (LIBs) have been the dominant energy storage technology for mobile applications, and they are also considered as the most suitable technology for electric vehicles and stationary energy storage systems. $LiNi_xCo_yMn_{1-x-y}O_2$ (NCM)-based cathodes have attracted many attentions due to their high power/energy densities, low cost, and low toxicity. [4-8] It is commonly accepted that the energy density of NCM-based cathodes is directly proportional to the content of nickel when the cut-off potential is below 4.3 V (*vs.* Li/Li^+). However, when the cut-off potential is raised to 4.6 V (*vs.* Li/Li^+) or above, NCM622 becomes the top candidate with optimized specific energy density (see the comparison of specific energy density of Li-ion battery (based on cathode, **Fig. S1**) and good rate performance [9, 10], as Cui et al. and Xiao et al. find that NCM622 show the highest Li-ion diffusivity with the minimum temperature dependence. On the other hand, the gain on the specific energy density by raising the cut-off potential can be achieved at an expense on irreversible phase transition, transitional metal (TM) dissolution, oxygen evolution and parasitic interface reactions between the deeply delithiated NCM particles and electrolyte, resulting in accelerated loss of the electrochemical performance and severe safety hazard.[10-13]

Mitigating the parasitic reaction is an important means to improve the stability of NCM622 at high cut-off potential. Various strategies including reducing reaction area (single crystal, [14-21] morphology optimization [22-24]), reducing reactivity (doping [25, 26]) and isolating reactant (surface coating [27]) have been implemented to mitigate the performance decay when working with a high cut-off potential. Among these mitigation strategies, surface coating is a common and effective method. Besides oxide coating (Al_2O_3, ZnO, TiO_2 et al.), carbon-coated $LiFePO_4$ (LFP) is a good coating candidate for NCM owing to their stable surface chemistry, electronically and ionically conductive nature.[28-30] Pan et al. reported

that 10 wt% Nano-LFP particle coating significantly improved the cycling stability of NCM523 between 3.0-4.6 V *vs.* Li/Li^+.[28] Wan et al. also prepared nano-LFP particles coated NCM811 and achieved a stable cycling performance between 3.0-4.3 V *vs.* Li/Li^+.[29] The surface coating is mostly considered as physically stable barrier layer to block the direct contact between the active electrode material and the electrolyte. Therefore, a good adhesion and completely coating between the NCM materials and the coating layers is generally pursued by adopting high temperature annealing to maximize the physical protection.[28, 29] However, are good adhesion and completely coating actually necessary for NCM cathode with high-voltage characteristics?

Capacity decay is closely related to the dissolution of transition metals, which must have its dissolution path. Choi et al. and Siegel et al. showed that the dissolution of Mn was anisotropic, and had crystal surface selectivity in $LiMn_2O_4$ cathode material, implying that the interfacial reactions have preferential active sites.[31, 32] Wang et al. also showed that the interface reactions between TM ions in NCM cathode and ethylene carbonate (EC) molecules are closely related to the cyclic stability of batteries.[33] Clarifying the reactive sites on the surface of NCM622 and performing targeted repairing can effectively improve the high-voltage stability of the material.

In this work, we present an effect interfacial modification of NCM622 with a "targeted mask". In detail, nano-$LiFePO_4$ (about 40 nm, along ac facet) plates were targetedly block the active sites on NCM622 (less than 30%) through a simple and fast mixing without any post-annealing. This targeted mask greatly improves NCM622 with both the cycle performances and thermal safety at a high charging cut-off potential at ≥4.6 V vs. Li/Li^+, unlocking the optimal specific energy density. Systematic *in/ex* situ characterizations, first-principles calculations and half/pouch cell evaluation prove that PO_4^{3-} is preferentially adsorbed on transition metal sites, stabilizing both the transition metal ions and oxygen ions on the surface against the ethylene carbonate-containing traditional electrolyte even under high voltage (≥

4.6 V *vs.* Li/Li^+). This study breaks free from traditional cognition on surface modification of NCM materials. Our findings may open up new venue for rational design of high-performance cathode materials through a low-cost and scalable decoration process, and reveal a new understanding of interfacial activity of materials.

2. Results and discussion

2.1 Structures of the LFPNP@C, NCM622 and NCM622@LFPNP@C powders

$LiFePO_4$@C nanoplates decorated NCM622 (denoted as NCM622@LFPNP@C) were synthesized by mixing 95 wt% NCM622 single-crystal particles and 5 wt% $LiFePO_4$@C nanoplates for 5 min at 2600 rpm in a high-speed mixer, as shown in **Fig. 1a**. The XRD patterns (in **Fig. S2**) of LFPNP@C nanoplates matches well with an olivine-type structure ($LiFePO_4$, PDF #40-1499), and the ratio of I(020)/I(200) is more than that of the standard, indicating preferred orientation of the LFPNP@C nanoplates along *ac* facet [34], [35] The characteristic XRD peaks of NCM622 and NCM622@LFPNP@C (**Fig. S2**) are well-indexed to the α-$NaFeO_2$ layer structure with space group of *R*-3*m*. No impurities can be detected, indicating that there is only physical interaction between NCM622 and LFPNP@C.

The morphologies of LFPNP@C, NCM622 and NCM622@LFPNP@C particles are characterized by SEM and TEM (**Fig. S3** and **Fig. 1)**. LFPNP@C presents plate-form morphology with the average thickness of about 40 nm (**Fig. S3**). Single-crystal NCM622 particles show smooth surface and average size of about 4 μm (**Fig. 1b** and **c**). The NCM622@LFPNP@C particles (**Fig. 1d** and **e**) are sprinkled with LFPNP@C. Further EDS mappings of the NCM622@LFPNP@C confirm the regional distributions of Fe and P on the surface of NCM622 (**Fig. 1f**), indicative of LFPNP@C locally decoration rather than a complete coating.

2.2 The effect of LFPNP@C decoration on electrochemical performance

As shown in **Fig. S1**, compared with NCM622, NCM811 delivers not far off energy densities when charged to 4.3 V, 4.6 V, 4.7 V and 4.8 V (*vs* Li/Li^+). However, high-Ni NCM are prone to deteriorated cycling performance (capacity and voltage), aggravated interphase degradation, and fatal thermal abuse at high potential (4.6 V, *vs* Li/Li^+), and these issues become more problematic with a higher Ni content.[36] There is no technological advantage to go with NCM811 at 4.6 V. Here we compare the energy densities (at the material level) of commercially available NCM811, NCM622 and NCM613 (**Fig. S5** and **Table S1**). The energy densities are calculated to be 780-790 Wh kg^{-1} for NCM811, 800-825 Wh kg^{-1} for NCM622 and NCM613, 800-810 Wh kg^{-1} for LFPNP@C decorated NCM622 and NCM613, respectively, inferring that the NCM622 and NCM613 cathode have higher energy density when charged to 4.6 V than the commercial NCM811 cathode charged to 4.3 V (*vs* Li/Li^+). The LFPNP@C decorated NCM622 shows a slightly lower energy density than the pristine NCM622, which is attributed to the relatively lower energy density than the NCM622 when charged to 4.6 V (*vs* Li/Li^+). Compared to other inactive coating like Al_2O_3 or TiO_2, the LFPNP@C decorated material is electrochemically active and is beneficial to reduce the loss of energy density due to coating, as confirmed by the plateau around 3.40 V during charge/discharge of NCM622@LFPNP (**Fig. S4**, charge/discharge profiles of NCM622@LFPNP@C|Li half-cell).

Fig. 2a-b shows the cycling performance of NCM622|Li and NCM622@LFPNP@C|Li at 0.5C and 1C in the voltage range of 2.7-4.6 V. It is obviously shown that the cycling stability is significantly improved when the pristine NCM622 is decorated by LFPNP@C nanoplates. A high reversible discharge capacity of 164 mAh g^{-1}, with capacity retention of 84.6%, is achieved by NCM622@LFPNP@C after 100 cycles at 0.5 C-rate (all cells were activated at 0.2C for three cycles). However, the discharge capacities of pristine-NCM622 declines at much faster pace and it remains only 128.2 mAh g^{-1} with 66% capacity retention after 100 cycles at 0.5 C-rate. Similarly, when the charging current increases to 1C (**Fig. 2b**),

the discharge capacity of NCM622@LFPNP@C decrease to 141.2 mAh g^{-1} after 200 cycles with 80.2% capacity retention, while the discharge capacity of pristine-NCM622 is almost close to 0 mAh g^{-1}. The charge-discharge curves of NCM622|Li and NCM622@LFPNP@C|Li cells at 1C at selected cycles are displayed in **Fig. 2c-d**. The voltage of pristine-NCM622|Li cell significantly degraded after 50 cycles. To further clarify the surface passivation effect of the LFPNP@C decoration, the cutoff voltage of NCM622|Li and NCM622@LFPNP@C|Li cells increases to 4.7 V and 4.8 V respectively (**Fig. S6 and S7**). NCM622@LFPNP@C still delivers obviously higher stability than NCM622 although both materials show obvious cracks after charged to 4.8 V, implying the LFPNP@C decoration can inhibit the parasitic surface reactions and reduce the capacity decay. The high precision leakage current measurement is the most effective way to quantitatively characterize the rate of parasitic reactions between the electrode materials and the electrolytes.[37, 38] **Fig. S8** compares the measured steady leakage current, which is an quantitative indicator of the electron transfer reaction across the cathode/electrolyte interface, for NCM622|Li and NCM622@LFPNP@C|Li cells held at 4.4, 4.5 and 4.6 V *vs*. Li/Li^+. The results clearly show that the decoration of LFPNP@C consistently suppresses the parasitic reaction on NCM622 at high potential, implying a better high-potential stability. All the results suggest that the high-voltage cycling performance of the NCM622 can be effectively improved through the LFPNP@C decoration. The synthesized procedures, coating materials and electrochemical performance of the NCM622 here are also compared with the best data reported in the literature (**Table 1**), confirming the simple, fast decoration approach presented in this work is significantly effective in protecting the NCM622 from attacking by the electrolyte components.

To determine exactly which composition in LFPNP@C acts to modify the interfacial failure behavior, samples with (NCM622@LFPNP@C) and without carbon (NCM622@LFPNP) decorated are compared at room temperature and 45℃, as shown in **Fig.**

S9. It can be observed that both two samples deliver much-improved stability (87.8% and 84.2% capacity retention after 60 cycles at 1 C-rate for NCM622@LFPNP and NCM622@LFPNP@C) than pristine-NCM622 (with 67.4% capacity retention) at 45℃ (**Fig. S9b**), indicates that the presence of carbon on the LFPNP is not necessary to improve the interface stability of NCM622. Also, pristine LFP performs poorly and can only release 52.8 mAh g^{-1} at 0.2C in the voltage range of 2.7-4.6 V at room temperature, such a poor LFP as a coating layer causes the obvious capacity loss from 202 mAh g^{-1} to 194 mAh g^{-1} at 0.2C. Therefore, the carbon only facilitates LFP utility in term of capacity.

To further validate the electrochemical performance in large-format cells, NCM622|Gr and NCM622@LFPNP@C|Gr pouch cells (~4.5 Ah) were assembled and cycled in the voltage range of 2.75–4.55 V at 1C. **Fig. 2e** shows their cycling performances; both cells maintained good stability up to 500 cycles. Subsequently, NCM622|Gr cell fades quickly and the discharge capacities is almost close to 0 mAh g^{-1} after 530 cycles, accompanied by significant swelling (inset in **Fig. 2e**). In contrast, NCM622@LFPNP@C|Gr cell maintains a good cycling stability with a capacity retention of 86.5% after 1000 cycles. The seriously degradation on cycle performance of the pristine NCM622 full cell may be attributed to the parasitic reactions and detrimental phase transition at high charging voltages (≥4.6 V).[39] Detailed characterization and discussion will be conducted in the following section.

2.3 The effect of LFPNP@C decoration on structural evolution during charge-discharge

In-situ XRD was used to investigate the phase transition behaviors of NCM622 and NCM622@LFPNP@C during charge-discharge. The (003) and (110) peaks that indicate *c*-axis and *a*-axis lattice parameters are shown in **Fig. 3** and **Fig. S10**. It can be observed that the pristine-NCM622 (**Fig. 3a**) and NCM622@LFPNP@C (**Fig. 3c**) show similar phase evolution over the initial charge-discharge process. The (003) diffractions of both cathodes shift to lower angle at initial charge stage and subsequent shifted to higher angle when

charged to above 4.1 V, corresponding to the initial expansion and subsequent sharp contraction along the *c*-axis. The unit cell shrinkage along the *a*-direction is nearly identical for the two cathodes. Specifically, the *c*-axis and *a*-axis lattice parameter variation (*Δc, Δa*) during charge process are calculated to be ~1.26% (*Δc*), ~1.94% (*Δa*) for NCM622 and ~1.21% (*Δc*), ~1.85% (*Δa*) for NCM622@LFPNP@C (**Fig. 3b and d**), respectively. The maximum *ΔV* (the unit cell volume change) of the two samples are calculated to be ~5.05% and ~4.85%. Apparently, NCM622@LFPNP@C shows smaller volume changes than NCM622, suggesting that the phase transition process of NCM622@LFPNP@C may be influenced by interfacial side reactions or interfacial side reaction products due to the targeted active-site protection.

2.4 Structural and interface chemistry after cycling

The NCM622 and NCM622@LFPNP@C cathodes are harvested from the pouch cells after 1000 cycles to investigate the potential impact of repeating cycling on structural evolution (**Fig. 4**). The (003) peak of pristine-NCM622 shifts from 18.855° to 18.582° (*Δ2θ*=0.273°) after 1000 cycles, while the value of *Δ2θ* for NCM622@LFPNP@C is only 0.02°, indicates more severe increase in interlayer lattice parameter *c* of pristine-NCM622 than the NCM622@LFPNP@C after long cycling. Moreover, some peaks corresponding to highly-delithiated phase ($Li_{0.13}Ni_{0.6}Co_{0.2}Mn_{0.2}O_2$) can be detected.[22, 40] This coincides with the observation that charging capacities are always higher than the discharging capacities at 500-540th cycle (**Fig. S11**). Visible structural damage can also be observed with SEM, as shown in **Fig. 4b, c**. The cycled NCM622@LFPNP@C well preserves the single-crystalline morphology at aggressive C-rates (1C, **Fig. 4c and Fig. 4e**) and voltage range (2.75-4.55 V *vs*. graphite/lithiated graphite), whereas significant amounts of lateral cracks in pristine-NCM622 particles (the red circles in **Fig. 4b**) can be observed. Furthermore, a Ni-rich rock-salt layer on the surface of cycled NCM622 (at 1000th cycle) can be obviously observed (**Fig. 4d**), which

further suggests that the cycled cathode experienced sever crystalline stress and the subsequent corrosion by electrolyte.[41]

The cathode/electrolyte interface is the location for charge transfer and parasitic reactions. The electrochemical impedance variations of NCM622|Li and NCM622@LFPNP@C|Li half cells during cycling were deconvoluted and quantified by electrochemical impedance spectroscopy, as shown in **Fig. 4f**. The obtained Nyquist plots generally consist of two semicircles, corresponding to the surface film resistance (R_s) and the charge-transfer resistance (R_{ct}), respectively. After 10 cycles, the R_{ct} of pristine-NCM622 is much larger than that of NCM622@LFPNP@C (**Fig. 4f**). The increase is generally related to the microstructural degradation and loss of particle contact, as described by Muto et al., [42] as well as the accumulation of poorly conductive parasitic products such as LiF, Li_2CO_3 and $LiFPO_x$ on the surface of the pristine-NCM622.[43] However, NCM622@LFPNP@C cathode shows suppressed impedance increase, as shown in **Fig. 4f**. This significant difference indicates that LFPNP@C decoration reduces the surface fading due to parasitic reactions between NCM622-cathode and electrolyte.

Apart from the accumulation of CEI (cathode electrolyte interphase) during cycling, TM cation dissolution is another notorious reason for capacity decay. The dissolved TM cations can migrate to the anode through the electrolyte, leading to SEI deterioration and then shortened lifetime. [44] The corresponding EDS of cycling graphite are demonstrated in **Fig. S12**, Ni, Co and Mn, either as cation or metal, can be clearly detected on the graphite particles from NCM622|Graphite pouch cell, whereas only trace Mn element are detected on the graphite particle from NCM622@LFPNP@C|Graphite pouch cell, confirming that the LFPNP@C decoration is stable and sufficiently robust to provide long-term protection of NCM622. The transition metal cation dissolution after 1000 cycle at 1C is further characterized by inductively coupled plasma-atomic emission spectrometer (ICP-AES) and

compared in **Fig. 4g**. It is found that the LFPNP@C decoration significantly mitigating the dissolution of transition metal cations.

Since the capacity of NCM622|graphite pouch cell fades quickly, accompaning by gas bulging (inset in **Fig. 2e**), the gas is analyzed by gas chromatography (**Fig. S13** and **Table S2)**. H_2, CH_4, C_2H_4, C_2H_6, C_3H_8 and C_4H_{10} are detected, and H_2 is the dominant species among these gases. These reductive species originate from the deteriorated electrolytes due to interface reactions with deeply delithiated cathode. The difference in the volume of gas evolution between NCM622@LFPNP@C and pristine-NCM622 indicates that the LFPNP@C decoration significantly mitigates the parasitic reaction between electrode and electrolyte in the high cut-off voltage (≥4.6 V).

2.5 Thermal stability of NCM622 and NCM622@LFPNP@C and the thermal runaway behaviors of their batteries

The safety of NCM-battery is of great significance, while the thermostability of cathode materials highly contribute to the battery safety. The delithiated NCM cathode can release oxidizing species (O_2, O_2^-, O^-, et al.) during the heating process due to phase transition, triggering highly exothermic reactions with the anode or electrolyte, and leading to severe thermal runaway.[45] The DSC curves (**a**) and O_2 spectra of the delithiated NCM622 and NCM622@LFPNP@C at 4.3 V (**b**) are measured from 30 °C to 600 °C, as shown in **Fig. 5**. Compared to the pristine-NCM622, NCM622@LFPNP@C exhibits a higher onset temperature for both heat release and oxygen evolution (293.1 °C), and phase transition from spinel-type to rock-salt (462.7 °C). It is also observed that NCM622@LFPNP@C releases less O_2 during the thermal ramping. Both the thermal analysis and O_2 evolution results suggest that NCM622@LFPNP@C is thermally more stable than its pristine counterpart. The *in situ* heating XRD patterns also confirm that the highly delithiated NCM622@LFPNP@C (**Fig. S14**) shows even better thermal stability than commercial NCM811 (4.2V, *vs.* grapgite).[46]

To further illustrate the positive impact of LFPNP@C decoration, ARC tests are conducted on NCM622 and NCM622@LFPNP@C pouch cells with OCV(open circuit voltage) of 4.55 V, as shown in **Fig. 5c**. Three critical temperatures, T_1, T_2 and T_3, are derived from the ARC test results to evaluate the thermal safety of lithium-ion battery.[47] T_1 is denoted as the onset temperature of self-heating, where the battery temperature rising rate exceeds 0.02 °C min^{-1}. The main reason for battery self-heating is ascribe to the failure of the solid-electrolyte interphase (SEI).[48] T_2 is the onset temperature of thermal runaway and is defined as the temperature at which the battery temperature rate exceeds 1 °C s^{-1}. T_3 is the maximum temperature.[47, 49] Higher T_1, T_2 and lower T_3 are considered to represent better thermal safety.[46] As shown in **Fig. 5c**, T_1 for pristine-NCM622|Gr and NCM622@LFPNP@C|Gr cells are 91.4 °C and 92.8 °C, and T_2 is around 204 °C for pristine-NCM622|Gr and 212 °C for NCM622@LFPNP@C|Gr. T_3 is 570°C for pristine-NCM622|Gr and 415°C for NCM622@LFPNP@C|Gr, indicative of better thermal safety of NCM622@LFPNP@C|Gr than pristine-NCM622|Gr. According to the thermal reaction mechanism on NCM-based LIBs, oxidizing species (O_2, O_2^-, O^-, et al.) released by NCM material at high temperature play essential role at T_2 and T_3.[46] Then combining the ARC, STA-MS and *in-situ* heating XRD results, we believe that the better thermal safety of NCM622@LFPNP@C|Gr can be attributed to the interface passivation of NCM622 by LFPNP@C decoration.

2.6 First-principles calculations of adsorption site and interfacial stability

Based on the fact that LFPNP@C is only locally adsorbed on the NCM622 surface, we try to explore the modification mechanism of LFPNP@C on NCM622 for high-voltage stability. Three different PO_4^{3-} absorption sites on the most stable crystal planes NCM622(104) (**Fig. S15**) are considered for structure optimization (**Fig. 6a**): (1) oxygen sites, (2) transition metal sites, (3) lithium sites. The optimized PO_4^{3-}/NCM622(104) structure and adsorption total energy are calculated and compared in **Fig. 6b, e**. The optimized absorption sites, which

have the lowest total energy, are transition metal and lithium sites (-818.39 eV), followed by transition metal sites (-817.66 eV), and finally lithium sites (-817.65 eV), inferring that the PO_4^{3-} is preferentially adsorbed on transition metal sites.

Oxygen evolution and TM dissolution are considered to be the main reasons for NCM cathode decay, which is highly related with the interface reactions between TM ions and EC molecules. The oxygen evolution will be initiated during the delithiation of NCM materials, which followed by cation migration to the Li-layer, result in irreversible phase transition.[39] This phase transformation cause capacity or rate capability fading. Hence, possible interfacial decomposition reactions before and after introducing the LFPNP@C decorating layer are explored by calculating the O^{2-} vacancy formation energy (**Fig. 6f**). The molecular formula of NCM622 after charged to 4.6 V *vs* Li/Li^+ is calculated to be $Li_{0.13}Ni_{0.6}Co_{0.2}Mn_{0.2}O_2$, according to the initial charge capacity. Then the vacancy formation energies of O^{2-} in pristine-$Li_{0.13}Ni_{0.6}Co_{0.2}Mn_{0.2}O_2$ and $Li_{0.13}Ni_{0.6}Co_{0.2}Mn_{0.2}O_2$@LFPNP@C are calculated and compared (**Fig. 6f**). **Fig. 6f** reveals that the O^{2-}-vacancy formation energy of pristine $Li_{0.13}Ni_{0.6}Co_{0.2}Mn_{0.2}O_2$ is negatively very low (-5.68 eV), suggesting that the NCM622 surface is very unstable when charging to 4.6 V vs Li/Li^+. However, the interface stability of NCM622@LFPNP@C can be evidently enhanced when coated with $FePO_4$ layer. The inside and outside O^{2-}-vacancy formation energies of $Li_{0.13}Ni_{0.6}Co_{0.2}Mn_{0.2}O_2/FePO_4$ increase to -5.18 and -4.68 eV, respectively, inferring restrained dissolution of oxygen from charged-NCM622 by LFPNP@C decoration. Previously, Prof. Tobias Placke et al proposed that Li_3PO_4 in the electrolyte acted as a transition metal capture agent and adsorbed the dissolved Ni^{2+}, Co^{2+} and Mn^{2+}, hence reducing TM crossover to the anode and hindering SEI deterioration.[50] Similarly, the targeted $FePO_4$ decoration may also serve as a "stabilizer", decrease the interface reactions between TM ions and EC molecules, finally improves the stability of cathode/electrolyte interface.

3. Conclusion

In this work, stability of NCM622 at high-voltage is managed by masking the active sites on the surface, then tradition cognitions on surface coating and interface modification are refreshed. This targeted masking is proved to greatly improve both the cycle performances and thermal safety of NCM622 at a high charging cut-off potential at ≥4.6 V *vs.* Li/Li^+. First-principal calculations and *in situ/ex situ* structural characterizations indicate that PO_4^{3-} tends to be preferentially adsorbed on transition metal sites, stabilize the transition metal ions and oxygen ions against EC-containing electrolyte even under high voltage (≥ 4.6 V *vs.* Li/Li^+). Besides the parasitic reactions, detrimental O3/H1-3 phase transition of commercial NCM622 during cycling is also suppressed by the targeted masking. The mechanistic study implies that the importance of surface chemistry modification, achieved by targeted masking in this work, outweighs that of physical protection achieved by thick and wide coverage of surface coating strategies. Our new findings may open up new venues for rational design on electrolyte/electrode interface chemistry, shedding light on a new way to achieve designed NCM622 cathode with high-voltage characteristics.

4. Experimental Section

Material synthesis: NCM622 single-crystal particles were provided by Beijing Easpring Material Technology Co. Ltd, China. Crystal orientation tuning of $LiFePO_4$ nanoplates were synthesized by previous solvothermal process.[29] Specifically, 7.56 mol $LiOH·H_2O$ was introduced to 14.4 L ethylene glycol under stirring, then slowly added 4.2 mol H_3PO_4 into the LiOH solution to form a white suspension. After the neutralization reaction, 2.8 mol $FeSO_4·7H_2O$ was added under stirring to form a viridescent suspension. The mixtures were then transferred into a 20 L steel reactor and heated to 180 °C for 10 h. After cooled down to room temperature, the obtained gray-green precipitates were washed with deionized water and ethanol. To achieve carbon coating, $LiFePO_4$ nanoplates were mixed in an agate jar with 10 wt % polyvinyl alcohol (PVA, with a polymerization degree of 1700) and then calcined in a

furnace at 650 °C for 3 h in N_2 atmosphere to obtain $LiFePO_4$@C nanoplates (~400 g, denoted as LFPNP@C). $LiFePO_4$@C nanoplates coated NCM622 (denoted as NCM622@LFPNP@C) were synthesized by mixing 95 wt% NCM622 single-crystal particles and 5 wt% $LiFePO_4$@C nanoplates with high-speed mixer (2600 rpm) for 5 min through electrostatic interactions. Similarly, the pristine LFP coated NCM622 (without carbon coating, NCM622@LFPNP) were synthesized to confirm the effect of carbon.

XRD and SEM characterization: The crystalline structure of LFPNP@C, NCM622 and NCM622@LFPNP@C were analyzed by X-ray diffraction (XRD, Bruker) with Cu Kα radiation over the 2θ angles from 10º to 70°. *In situ* XRD measurements were also performed to characterize the structural changes of NCM622 cathodes during charging/discharing, using a specially designed cell equipped with an X-ray-transparent berylium window (Bruker). The *in situ* XRD patterns were collected over the 2θ angles from 10-70° on charging and discharging at a current rate of 0.1 C (1C=180 mA g^{-1}). *In situ* heating synchrotron high-energy X-ray diffraction (HEXRD) was also carried out at sector of 11-ID-C of Advanced Photon Source (APS) with a wavelength of 0.1173Å, to investigate the thermal stability of the NCM622 cathodes. The charged cathode was collected from the fully charged battery (4.6V). A capillary furnace was used to heat the cathode powder from 30 °C to 500 °C at a heating rate of 10 °C min^{-1}. The obtained 2D diffraction patterns from a PerkinElmer amorphous silicon detector were converted to 1D patterns. Their morphologies were observed with a scanning electron microscope (SEM, Zeiss Gemini SEM 300) and a transmission electron microscope (TEM, JEOL 2100 Plus). The elemental compositions were analyzed with an energy-dispersive X-ray spectrometer (EDS) attached to the SEM instrument.

Half-cell assembly: The NCM622|Li and NCM622@LFPNP@C|Li half-cell tests were conducted using coin-type half-cells (CR2032 size) assembled in an argon-filled glove box

(Mikrouna Super 1220). The working electrodes were prepared by casting the slurry of active material (80 wt%), conductive carbon black C45 (10 wt%) and polyvinylidene fluoride (10 wt%) on an aluminium foil, followed by drying at 80 °C in a vacuum overnight. The loading of active material was controlled to between 4.0 and 5.0 mg cm^{-2}. The electrolyte was 1 M $LiPF_6$ in ethylene carbonate (EC)/dimethyl carbonate (DMC)/ethyl methyl carbonate (EMC) (1:1:1, *v*/*v*/*v*) with 1.0 wt% vinylene carbonate (VC) additive, while a micro-porous film Celgard 2400 polypropylene membrane was the separator and lithium foil were used as the counter electrode.

Full-cell assembly: The NCM622|graphite and NCM622@LFPNP@C|graphite full-cell tests were conducted using stacked pouch cells (4.5 Ah) assembled in a dry room. The cathode electrodes were prepared by coating the mixture slurry of active material (96 wt%), super P (1.5 wt%), carbon nanotubes (1 wt%) and polyvinylidene fluoride (1.5 wt%) on an aluminium current collector, followed by drying at 120 °C in a vacuum for 10 h. The areal capacity was controlled to between 5.6 and 6.0 mAh cm^{-2}. The anode electrodes were composed of graphite (96.8 wt%), super P (0.7 wt%), carboxy methyl cellulose sodium (1 wt%) and styrene butadiene rubber (1.5 wt%), and fabricated following the same coating and drying procedures. The capacity ratio between negative electrode and positive electrode was controlled to between 1.08 and 1.1 (based on 4.6 V of NCM622|Li coin cell). Al_2O_3-coated polyethylene film was used as the separator. The specific characteristics of NCM622|graphite and NCM622@LFPNP@C|graphite full-cell were shown in **Table S3**.

Electrochemical measurements: The galvanostatic charge–discharge characteristics of half-cell were carried out using a Land CT2001A battery test system in a voltage range of 2.7–4.6 V, 2.7-4.7 V and 2.7-4.8 V at various C rates at room temperature and 45°C. The cycling performance of full batteries were charged and discharged between 2.75 and 4.55 V at

room temperature. The electrochemical impedance spectroscopy (EIS) of the half-cells were evaluated on a CHI660e electrochemical work station (Chenhua Co. Ltd). A high precision leakage current measuring system at Argonne National Laboratory was used to obtain the leakage current for electrodes holding at 4.4, 4.5 and 4.6 V at room temperature (25±2 °C).

Inductively coupled plasma (ICP) and gas chromatography (GC) measurement: For metal dissolution during cycling, anode powders harvested from post-test (1000 cycles) pouch cells were disassembled and wash several times with DMC in the glovebox. The organic solution was collected for HNO_3 acid digestion and test the supernatant (X Series, Thermo). The GC were measured by SHIMADZU GC-2014.

Simultaneous thermal analyzer - mass spectrometry (STA-MS) test: The STA-MS test was used to examine the thermostability of the cathode by a Netzsch STA 449 F5 Jupiter coupled with QMS 403 D Aëolos. The samples were obtained by disassembling a fully charged cell (4.3 V) in a glovebox. The cathode powder was scraped from electrode after having been rinsed several times with DMC to scour lithium salt ($LiPF_6$) in the electrode. Then as-prepared samples were dried in argon before test. For the STA-MS measurement, about 4.0 mg powder was placed in an aluminum crucible and then heated from 30 °C to 600 °C (20 °C min^{-1}) to probe potential heat generation, with the gas generation characterized by the mass spectrometry.

Accelerated rate calorimetry (ARC) test: The safety of the full cell was evaluated using an extended volume accelerated rate calorimetry (EV-ARC) manufactured by Thermal Hazard Technology (THT). Before thermal runaway tests, the batteries were fully charged to 4.55 V at 0.5 C. Two batteries were wrapped together, and type K thermocouples were placed between the two batteries to monitor the internal temperature. The ARC tests were performed

with the heat-wait-seek method to ensure an adiabatic condition, with a heating step of 5 °C, waiting time of 45 min, and self-heating rate of 0.02 °C min^{-1}.

First-Principles Calculations: The fundamental mechanism of one PO_4^{3-} absorbed on NCM622(104) surface was investigated. The PO_4^{3-} /NMC622(104) structure consisted of 36Li, 22Ni, 7Co, 7Mn, 76O and 1P atoms. Three different PO_4^{3-} absorption sites on NCM622(104) surfaces were considered during structure optimization. The Van der Waals interactions were considered using the DFT-D3 method with Becke-Jonson damping.

The density functional theory calculations were performed with Vienna Ab initio Simulation Package (VASP) code.[51] The Perdew-Burke-Ernzerhof (PBE) was used to approximate the exchange-correlation functional. The projectoraugmented wave (PAW) method [52-54] was used for electron and core interaction. The Hubbard U parameter was used for transition metal in NCM622 and $FePO_4$ to correct the delocalization of the d-orbital. The U values for Ni, Co, and Mn (6.7, 4.91, and 4.64, respectively) were selected from reported value. [55] The U value for Fe is 4.64. The pristine NCM622 included 6Li, 10Mn, 10Co, 28Ni and 96O. The $FePO_4$ coated NCM622 structure consisted of 6Li,10Mn, 10Co, 28Ni, 4Fe, 4P and 112O. The cutoff energy was set for 520 eV. The convergence criteria in the electronic self-consistent iterations were 10^{-5} eV and the convergence criteria for ionic relaxation was set to be 0.01 eV/Å, respectively.

The transition metal (M) Ni, Mn, Co vacancy formation energy was described as follows:[56]

$$E_F = E\,[Li_xM_{y-1}O_z] - E\,[Li_xM_yO_z]) + u_M$$

Where E_F was the M vacancy formation energy, and u_M was the chemical potential of M.

The O vacancy formation energy was defined as follows:[57]

$$E_F = E\,[Li_xM_yO_{z-1}] - E\,[Li_xM_yO_z]) + 1/2E_{O2}$$

Where $E[Li_xM_yO_{z-1}]$, $E[Li_xM_yO_z]$ and E_{O2} were the total energies of $Li_xM_yO_{z-1}$, $Li_xM_yO_z$ and the gas phase of O_2, respectively.

All simulation works were performed using the computing resources at National Supercomputing Center in Shenzhen.

CRediT authorship contribution statement

Qiao Hu: Conceptualization, Methodology, Investigation, Formal analysis, Writing-original draft. **Yufang He:** Investigation. **Dongsheng Ren:** Resources, Formal analysis. **Youzhi Song:** Resources, Formal analysis. **Yanzhou Wu:** Formal analysis, Investigation. **Hongmei Liang:** Formal analysis. **Jinhui Gao:** Methodology. **Gang Xu:** Supervision. **Jiyu Cai:** Supervision. **Tianyi Li:** Investigation. **Hong Xu:** Writing-review & editing. **Li Wang:** Conceptualization, Methodology, Investigation, Writing-review & editing. **Zonghai Chen:** Conceptualization, Supervision, Writing-review & editing. **Xiangming He:** Conceptualization, Supervision, Project administration, Funding acquisition.

Declaration of competing interest

The authors declare that they have no known competing financial interests or personal relationships that could have appeared to influence the work reported in this paper.

Acknowledgements

We would like to show gratitude to the National Natural Science Foundation of China (No. U21A20170(X. He), 52007099(D. Ren) and 52073161(H. Xu)), the Ministry of Science and Technology of China (No. 2019YFE0100200(X. He) and 2019YFA0705703(L. Wang)) and the Tsinghua University Initiative Scientific Research Program (No. 2019Z02UTY06(X. He)). Research at Argonne National Laboratory was supported by U.S. Department of Energy (DOE), Vehicle Technologies Office. Argonne National Laboratory is operated for the US Department of Energy by U Chicago Argonne, LLC, under contract DE-AC02-06CH11357. The authors also thank Tsinghua University-Zhangjiagang Joint Institute for Hydrogen Energy and Lithium Ion Battery Technology, thank Kelong New Energy.

Received: ((will be filled in by the editorial staff))
Revised: ((will be filled in by the editorial staff))
Published online: ((will be filled in by the editorial staff))

Appendix A. Supporting information

Supplementary data associated with this article can be found in the online version at doi:10.1016/j.nanoen.

References

[1] M.S. Whittingham, Ultimate Limits to Intercalation Reactions for Lithium Batteries, Chem. Rev., 114 (2014) 11414−11443.
[2] J.B. Goodenough, Evolution of Strategies for Modern Rechargeable, Accounts of chemical Research, 46 (2013) 1053–1061.
[3] N. Nitta, F. Wu, J.T. Lee, G. Yushin, Li-ion Battery Materials: Present and Future, Materials Today, 18 (2015) 252-264.
[4] X. Fan, G. Hu, B. Zhang, X. Ou, J. Zhang, W. Zhao, H. Jia, L. Zou, P. Li, Y. Yang, Crack-Free Single-Crystalline Ni-Rich Layered NCM Cathode Enable Superior Cycling Performance of Lithium-Ion Batteries, Nano Energy, 70 (2020).
[5] M.S. Whittingham*, Lithium Batteries and Cathode Materials, Chem. Rev., 104 (2004) 4271-4302.
[6] H.K. Bruce Dunn, Jean-Marie Tarascon, Electrical Energy Storage for the grid a battery of choice, Science, 334 (2011) 928-935.
[7] Y. Song, X. Liu, D. Ren, H. Liang, L. Wang, Q. Hu, H. Cui, H. Xu, J. Wang, C. Zhao, X. Zuo, G.L. Xu, K. Amine, X. He, Simultaneously Blocking Chemical Crosstalk and Internal Short Circuit via Gel‐Stretching Derived Nanoporous Non-Shrinkage Separator for Safe Lithium-Ion Batteries, Adv. Mater., (2021) 2106335.
[8] S. Zhang, J. Ma, Z. Hu, G. Cui, L. Chen, Identifying and Addressing Critical Challenges of High-Voltage Layered Ternary Oxide Cathode Materials, Chem. Mater., 31 (2019) 6033-6065.
[9] S. Cui, Y. Wei, T. Liu, W. Deng, Z. Hu, Y. Su, H. Li, M. Li, H. Guo, Y. Duan, W. Wang, M. Rao, J. Zheng, X. Wang, F. Pan, Optimized Temperature Effect of Li-Ion Diffusion with Layer Distance in $Li(Ni_xMn_yCo_z)O_2$ Cathode Materials for High Performance Li-Ion Battery, Adv. Energy Mater., 6 (2016).
[10] P. Xiao, T. Shi, W. Huang, G. Ceder, Understanding Surface Densified Phases in Ni-Rich Layered Compounds, ACS Energy Letters, 4 (2019) 811-818.
[11] Q. Zhang, K. Liu, C. Li, S. Tan, L. Li, X.-G. Sun, W. Li, X. Liu, J. Zhang, S. Dai, The Surface Triple-Coupling on Single Crystalline Cathode for Lithium Ion Batteries, Nano Energy, 86 (2021).
[12] F. Lin, D. Nordlund, Y. Li, M.K. Quan, L. Cheng, T.-C. Weng, Y. Liu, H.L. Xin, M.M. Doeff, Metal Segregation in Hierarchically Structured Cathode Materials for High-Energy Lithium Batteries, Nat. Energy, 1 (2016).
[13] T. Or, S.W.D. Gourley, K. Kaliyappan, A. Yu, Z. Chen, Recycling of Mixed Cathode Lithium-Ion Batteries for Electric Vehicles: Current Status and Future Outlook, Carbon Energy, 2 (2020) 6-43.
[14] T. Kimijima, N. Zettsu, K. Yubuta, K. Hirata, K. Kami, K. Teshima, Molybdate Flux Growth of Idiomorphic $Li(Ni_{1/3}Co_{1/3}Mn_{1/3})O_2$ Single Crystals and Characterization of Their Capabilities as Cathode Materials for Lithium-Ion Batteries, J. Mater. Chem. A, 4 (2016) 7289-7296.
[15] J. Zhu, G. Chen, ingle-Crystal Based Studies for Correlating the Properties and High-Voltage Performance of $Li[Ni_xMn_yCo_{1-x-y}]O_2$ cathodes, J. Mater. Chem. A, 7 (2019) 5463-5474.
[16] S. Kuppan, Y. Xu, Y. Liu, G. Chen, Phase Transformation Mechanism in Lithium Manganese Nickel Oxide Revealed by Single-Crystal Hard X-ray Microscopy, Nat. Commun., 8 (2017) 14309.
[17] X. Xu, H. Huo, J. Jian, L. Wang, H. Zhu, S. Xu, X. He, G. Yin, C. Du, X. Sun, Radially Oriented Single-Crystal Primary Nanosheets Enable Ultrahigh Rate and Cycling Properties of

$LiNi_{0.8}Co_{0.1}Mn_{0.1}O_2$ Cathode Material for Lithium-Ion Batteries, Adv. Energy Mater., 9 (2019).
[18] H. Li, J. Li, X. Ma, J.R. Dahn, Synthesis of Single Crystal $LiNi_{0.6}Mn_{0.2}Co_{0.2}O_2$ with Enhanced Electrochemical Performance for Lithium Ion Batteries, J. Electrochem. Soc., 165 (2018) A1038-A1045.
[19] G. Conforto, R. Ruess, D. Schröder, E. Trevisanello, R. Fantin, F.H. Richter, J. Janek, Editors' Choice—Quantification of the Impact of Chemo-Mechanical Degradation on the Performance and Cycling Stability of NCM-Based Cathodes in Solid-State Li-Ion Batteries, J. Electrochem. Soc., 168 (2021).
[20] D. Mohanty, J. Li, S.C. Nagpure, D.L. Wood, C. Daniel, Understanding the Structure and Structural Degradation Mechanisms in High-Voltage, Lithium-Manganese–Rich Lithium-Ion Battery Cathode Oxides: A Review of Materials Diagnostics, MRS Energy & Sustainability, 2 (2015).
[21] W.S. Yoon, O. Haas, S. Muhammad, H. Kim, W. Lee, D. Kim, D.A. Fischer, C. Jaye, X.Q. Yang, M. Balasubramanian, K.W. Nam, In Situ soft XAS Study on Nickel-Based Layered Cathode Material at Elevated Temperatures: A Novel Approach to Study Thermal Stability, Sci. Rep., 4 (2014) 6827.
[22] F. Li, Z. Liu, J. Shen, X. Xu, L. Zeng, B. Zhang, H. Zhu, Q. Liu, J. Liu, M. Zhu, A Nanorod-Like Ni-Rich Layered Cathode with Enhanced Li^+ Diffusion Pathways for High-Performance Lithium-Ion Batteries, J. Mater. Chem. A, 9 (2021) 2830-2839.
[23] L. Zhang, N. Li, B. Wu, H. Xu, L. Wang, X.Q. Yang, F. Wu, Sphere-Shaped Hierarchical Cathode with Enhanced Growth of Nanocrystal Planes for High-Rate and Cycling-Stable Li-Ion Batteries, Nano Lett., 15 (2015) 656-661.
[24] Y.K. Sun, Z. Chen, H.J. Noh, D.J. Lee, H.G. Jung, Y. Ren, S. Wang, C.S. Yoon, S.T. Myung, K. Amine, Nanostructured High-Energy Cathode Materials for Advanced Lithium Batteries, Nat. Mater., 11 (2012) 942-947.
[25] C. Gong, W. Lv, L. Qu, O.E. Bankole, G. Li, R. Zhang, M. Hu, L. Lei, Syntheses and Electrochemical Properties of Layered $Li_{0.95}Na_{0.05}Ni_{1/3}Co_{1/3}Mn_{1/3}O_2$ and $LiNi_{1/3}Co_{1/3}Mn_{1/3}O_2$, J. Power Sources, 247 (2014) 151-155.
[26] L. Croguennec, J. Bains, J. Bréger, C. Tessier, P. Biensan, S. Levasseur, C. Delmas, Effect of Aluminum Substitution on the Structure, Electrochemical Performance and Thermal Stability of $Li_{1+x}(Ni_{0.40}Mn_{0.40}Co_{0.20-z}Al_z)_{1-x}O_2$, J. Electrochem. Soc., 158 (2011).
[27] H. Xie, Z. Liang, D. Luo, Y. Zhang, X. Ding, J. Cui, Z. Zhang, Z. Lin, A General Route of Fluoride Coating on the Cyclability Regularity of High-Voltage NCM Cathodes, Chem. Commun., 56 (2020) 12009-12012.
[28] Z. Wu, S. Ji, T. Liu, Y. Duan, S. Xiao, Y. Lin, K. Xu, F. Pan, Aligned Li(+) Tunnels in Core-Shell $Li(Ni_xMn_yCo_z)O_2$@$LiFePO_4$ Enhances Its High Voltage Cycling Stability as Li-ion Battery Cathode, Nano Lett., 16 (2016) 6357-6363.
[29] Z. Zhong, L. Chen, C. Zhu, W. Ren, L. Kong, Y. Wan, Nano $LiFePO_4$ coated Ni rich composite as cathode for lithium ion batteries with high thermal ability and excellent cycling performance, J. Power Sources, 464 (2020).
[30] L. Liu, X. Yan, Y. Wang, D. Zhang, F. Du, C. Wang, G. Chen, Y. Wei, Studies of the Electrochemical Properties and Thermal Stability of $LiNi_{1/3}Co_{1/3}Mn_{1/3}O_2$/$LiFePO_4$ Composite Cathodes for Lithium Ion Batteries, Ionics, 20 (2014) 1087-1093.
[31] J.S. Kim, K. Kim, W. Cho, W.H. Shin, R. Kanno, J.W. Choi, A Truncated Manganese Spinel Cathode for Excellent Power and Lifetime in Lithium-Ion Batteries, Nano Lett., 12 (2012) 6358-6365.
[32] N. Kumar, K. Leung, D.J. Siegel, Crystal Surface and State of Charge Dependencies of Electrolyte Decomposition on $LiMn_2O_4$ Cathode, J. Electrochem. Soc., 161 (2014) E3059-E3065.
[33] X. Wang, A. Wang, L. Wang, X. He, Double Shuttle Double Catalysis Mechanism for H_2 Evolution in LIBs, Infomat, submitted.

[34] L. Wang, X. He, W. Sun, J. Wang, Y. Li, S. Fan, Crystal Orientation Tuning of $LiFePO_4$ Nanoplates for High Rate Lithium Battery Cathode Materials, Nano Lett., 12 (2012) 5632-5636.
[35] K. Dokko, S. Koizumi, H. Nakano, K. Kanamura, Crystal Orientation, and Electrochemical Reactivity of $LiFePO_4$ Synthesized by the Hydrothermal Method at 443 K, J. Mater. Chem., 17 (2007) 4803-4810.
[36] Z.C. Qiang Xie, and Arumugam Manthiram, Unveiling the Stabilities of Nickel-Based Layered Oxide Cathodes at an Identical Degree of Delithiation in Lithium‐Based Batteries. Adv. Mater., 33 (2021) 2100804.
[37] X. Zeng, Xu, G. L., Li, Y., Luo, X., Maglia, F., Bauer, C., Lux, S. F., Paschos, O., Kim, S. J., Lamp, P., Lu, J., Amine, K., Chen, Z., Kinetic Study of Parasitic Reactions in Lithium-Ion Batteries: A Case Study on $LiNi_{0.6}Mn_{0.2}Co_{0.2}O_2$, ACS Appl. Mater. Interfaces, 8 (2016) 3446-3451.
[38] H. Gao, X. Zeng, Y. Hu, V. Tileli, L. Li, Y. Ren, X. Meng, F. Maglia, P. Lamp, S.-J. Kim, K. Amine, Z. Chen, Modifying the Surface of a High-Voltage Lithium-Ion Cathode, ACS Appl. Energy Mater., 1 (2018) 2254-2260.
[39] F. Zhang, S. Lou, S. Li, Z. Yu, Q. Liu, A. Dai, C. Cao, M.F. Toney, M. Ge, X. Xiao, W.K. Lee, Y. Yao, J. Deng, T. Liu, Y. Tang, G. Yin, J. Lu, D. Su, J. Wang, Surface Regulation Enables High Stability of Single-Crystal Lithium-Ion Cathodes at High Voltage, Nat. Commun., 11 (2020) 3050.
[40] Y.-H.R. S.-C. Yin, I. Swainson, and L. F. Nazar*, X-ray/Neutron Diffraction and Electrochemical Studies of Lithium De/Re-Intercalation in $Li_{1-x}Co_{1/3}Ni_{1/3}Mn_{1/3}O_2$ ($x = 0 \rightarrow 1$, Chem. Mater, 18 (2006) 1901-1910.
[41] J.T. Yujing, Yuqin Wu, Linze Li, Yaobin Xu, Enyuan Hu, Bingbin Wu, Jiangtao Hu, Chongmin Wang, Ji-Guang Zhang, Yue Qi, Jie Xiao, Reversible Planar Gliding and Microcracking in a Single-Crystalline Ni-rich Cathode, Science, 370 (2020) 1313-1317.
[42] S. Muto, K. Tatsumi, Y. Kojima, H. Oka, H. Kondo, K. Horibuchi, Y. Ukyo, Effect of Mg-Doping on the Degradation of $LiNiO_2$-based Cathode Materials by Combined Spectroscopic Methods, J. Power Sources, 205 (2012) 449-455.
[43] W. Liu, P. Oh, X. Liu, M.J. Lee, W. Cho, S. Chae, Y. Kim, J. Cho, Nickel-Rich Layered Lithium Transition-Metal Oxide for High-Energy Lithium-Ion Batteries, Angew Chem. Int. Ed. Engl., 54 (2015) 4440-4457.
[44] L. Huang, X. Chen, H. Mühlenbernd, H. Zhang, S. Chen, B. Bai, Q. Tan, G. Jin, K.-W. Cheah, C.-W. Qiu, J. Li, T. Zentgraf, S. Zhang, Three-Dimensional Optical Holography Using a Plasmonic Metasurface, Nat. Commun., 4 (2013) 1-8.
[45] G. L. Xu, Q. Liu, K.K.S. Lau, Y. Liu, X. Liu, H. Gao, X. Zhou, M. Zhuang, Y. Ren, J. Li, M. Shao, M. Ouyang, F. Pan, Z. Chen, K. Amine, G. Chen, Building Ultraconformal Protective Layers on Both Secondary and Primary Particles of Layered Lithium Transition Metal Oxide Cathodes, Nat. Energy, 4 (2019) 484-494.
[46] X.L. Yan Li, Li Wang, Xuning Feng, Dongsheng Ren, Yu Wu, Guiliang Xu, Languang Lu, Junxian Hou, Weifeng Zhang, Yongling Wang, Wenqian Xu, Yang Ren, Zaifa Wang, Jianyu Huang, Xiangfeng Meng, Xuebing Han, Hewu Wang, Xiangming He, Zonghai Chen, Khalil Amine, Minggao Ouyang, Thermal Runaway Mechanism of Lithium-Ion Battery with $LiNi_{0.8}Mn_{0.1}Co_{0.1}O_2$ Cathode Materials, Nano Energy, 85 (2021) 105878.
[47] D. Ren, X. Feng, L. Liu, H. Hsu, L. Lu, L. Wang, X. He, M. Ouyang, Investigating the Relationship between Internal Short Circuit and Thermal Runaway of Lithium-Ion Batteries under Thermal Abuse Condition, Energy Stor. Mater., 34 (2021) 563-573.
[48] Y. Li, X. Liu, D. Ren, H. Hsu, G.-L. Xu, J. Hou, L. Wang, X. Feng, L. Lu, W. Xu, Y. Ren, R. Li, X. He, K. Amine, M. Ouyang, Toward a High-Voltage Fast-Charging Pouch Cell with TiO_2 Cathode Coating and Enhanced Battery Safety, Nano Energy, 71 (2020) 104643 .
[49] X. Feng, S. Zheng, D. Ren, X. He, L. Wang, H. Cui, X. Liu, C. Jin, F. Zhang, C. Xu, H.

Hsu, S. Gao, T. Chen, Y. Li, T. Wang, H. Wang, M. Li, M. Ouyang, Investigating the Thermal Runaway Mechanisms of Lithium-Ion Batteries based on Thermal Analysis Database, Appl. Energy, 246 (2019) 53-64.
[50] H.P. Klein Sven, Henschel Jonas, Bärmann Peer, Borzutzki Kristina, Beuse Thomas, Wickeren Stefan, Heidrich Bastian, Kasnatscheew Johannes, Nowak Sascha, Winter Martin, Placke Tobias, On the Beneficial Impact of Li_2CO_3 as Electrolyte Additive in NCM523|Graphite Lithium Ion Cells Under High-Voltage Conditions. Adv. Energy Mater. 11 (2021) 2003756.
[51] G.K. J.HAFNER, The Vienna AB-Initio Simulation Program VASP An Efficient and Versatile Tool for Studying the Structural Dynamic and Electronic Properties of Materials, Properties of Complex Inorganic Solids, (1997) 69-82.
[52] K.B. John P. Perdew, Matthias Ernzerhof, Physical Review Letters, 77 (1996) 3865-3868.
[53] J.F. G. Kresse, Generalized Gradient Approximation Made Simple, Phys. Rev. B, 54 (1996) 11169-11185.
[54] J.F. G. Kresse, Efficient Iterative Schemes for ab Initio Total-Energy Calculations Using a Plane-Wave Basis Set, Comput. Mater. Sci., 6 (1996) 15-50.
[55] J.M. Lim, T. Hwang, D. Kim, M.S. Park, K. Cho, M. Cho, Intrinsic Origins of Crack Generation in Ni-rich $LiNi_{0.8}Co_{0.1}Mn_{0.1}O_2$ Layered Oxide Cathode Material, Sci. Rep., 7 (2017) 39669.
[56] Y. He, H. Pham, Y. Gao, R.L. Patel, S. Sarkar, X. Liang, J. Park, Discovery of an Unexpected Metal Dissolution of Thin-Coated Cathode Particles and Its Theoretical Explanation, Advanced Theory and Simulations, 3 (2020).
[57] W. Hu, H. Wang, W. Luo, B. Xu, C. Ouyang, Formation and Thermodynamic Stability of Oxygen Vacancies in Typical Cathode Materials for Li-Ion Batteries: Density Functional Theory Study, Solid State Ionics, 347 (2020).
[58] L. Liang, C. Wu, X. Sun, X. Sun, L. Hou, J. Sun, C. Yuan, Sur-/Interface Engineering of Hierarchical $LiNi_{0.6}Mn_{0.2}Co_{0.2}O_2$@$LiCoPO_4$@Graphene Architectures as Promising High-Voltage Cathodes toward Advanced Li-Ion Batteries, Adv. Mater. Interfaces, 4 (2017).
[59] J. Fu, D. Mu, B. Wu, J. Bi, X. Liu, Y. Peng, Y. Li, F. Wu, Enhanced Electrochemical Performance of $LiNi_{0.6}Co_{0.2}Mn_{0.2}O_2$ Cathode at High Cutoff Voltage by Modifying Electrode/Electrolyte Interface with Lithium Metasilicate, Electrochim. Acta, 246 (2017) 27-34.
[60] P. Yan, J. Zheng, J. Liu, B. Wang, X. Cheng, Y. Zhang, X. Sun, C. Wang, J. G. Zhang, Tailoring Grain Boundary Structures and Chemistry of Ni-Rich Layered Cathodes for Enhanced Cycle Stability of Lithium-Ion Batteries, Nat. Energy, 3 (2018) 600-605.
[61] Q. Fan, S. Yang, J. Liu, H. Liu, K. Lin, R. Liu, C. Hong, L. Liu, Y. Chen, K. An, P. Liu, Z. Shi, Y. Yang, Mixed-Conducting Interlayer Boosting the Electrochemical Performance of Ni-Rich Layered Oxide Cathode Materials for Lithium Ion Batteries, J. Power Sources, 421 (2019) 91-99.

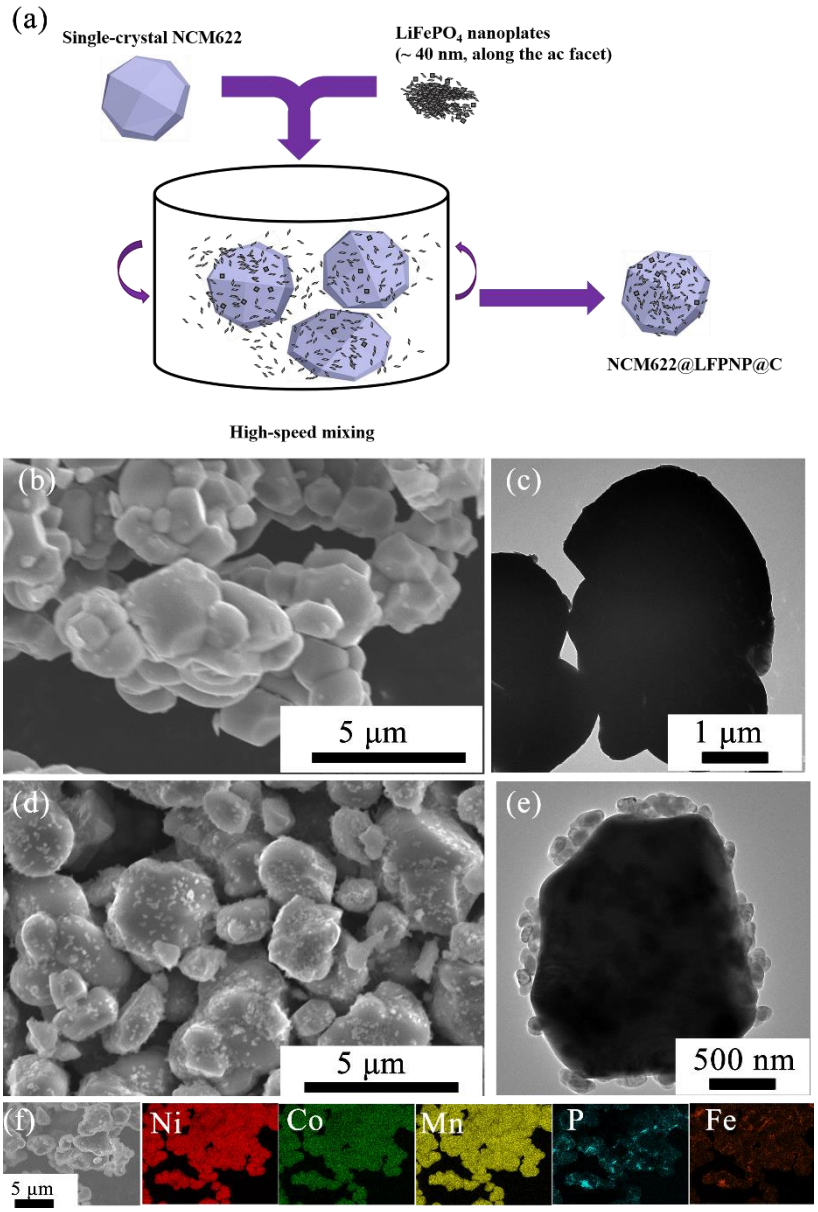

Fig. 1 Schematic of the preparation process for NCM622@LFPNP@C (a). Morphology and elemental distribution in pristine-NCM622 and NCM622@LFPNP@C. SEM images of NCM622 (b) and NCM622@LFPNP@C (d). TEM image of pristine-NCM622 (c) and NCM622@LFPNP@C (e). EDS mapping of NCM622@LFPNP@C (f).

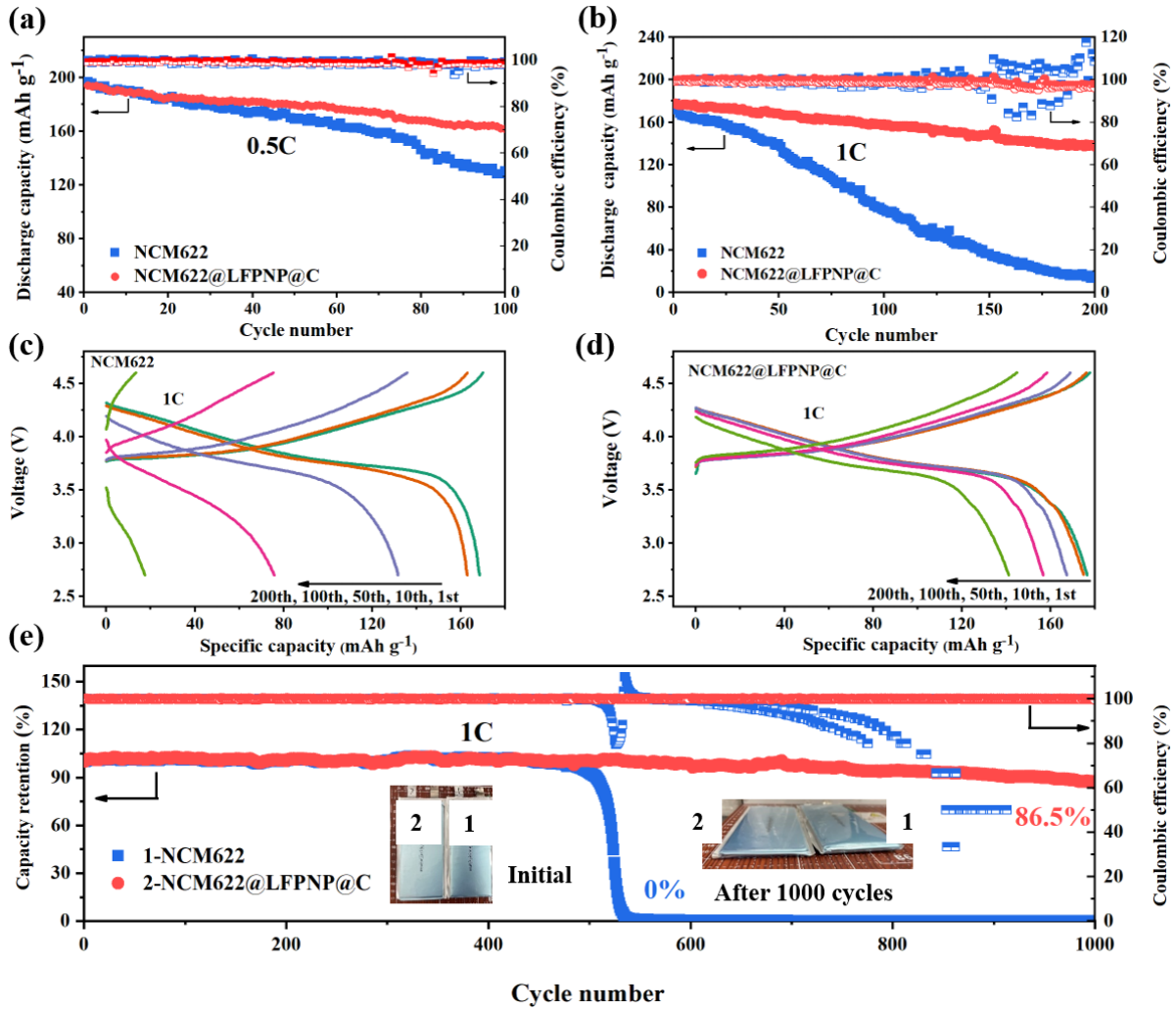

Fig. 2 The cycling performances of pristine-NCM622|Li and NCM622@LFPNP@C|Li half cells at 0.5C (a) and 1C (b) in the voltage range of 2.7-4.6V. Charge-discharge curves of NCM622 (c) and NCM622@LFPNP@C (d) half cells at 1C for the 1st, 10th, 50th, 100th and 200th cycle. (e) Cycling performances of pristine-NCM622|graphite and NCM622@LFPNP@C|graphite pouch cells (~4.5 Ah) at 1C (1C=180 mA g^{-1}) in the voltage range of 2.75-4.55 V. The inserted photographs show the pouch cells after formation (initial) and 1000 cycles. Flatulence can be observed for the pristine NCM622|graphite cell after 1000 cycles.

Table 1 The comparison of the electrochemical performance of NCM-based electrodes in this work and the existing literature.

Coating method	Coating amount (wt%)	Coating material	Cycling performance	Ref.
Physical mixing for 5 h at 500 rpm, then anneal at 100 °C	5	$LiFePO_4$ particles coated NCM523	82.3% for 150 cycles at 1/3C (2.7-4.6 V, NCM523|Li)	[28]
Sol-gel, then anneal at 650 °C	5	$LiCoPO_4$ and graphene coated NCM622	83% for 150 cycles at 1C (2.7-4.6 V, NCM622|Li)	[58]
Physical mixing for 1 h	2	Li_2SiO_3 coated NCM622	73.4% for 200 cycles at 1C (2.7-4.6 V, NCM622|Li)	[59]
Physical mixing for 10 min at 2000 rpm	5	$LiFePO_4$ particles coated NCM811	91.68% for 100 cycles at 1C (3.0-4.2 V, NCM811|Gr)	[29]
ALD, then anneal at 600 °C	coating layer: 10 nm	Li_3PO_4 coated NCM811	91.6% for 200 cycles at 1/3C (2.7-2.5 V, NCM811|Li)	[60]
Liquid mixing, then anneal at 500 °C	2	Li_3PO_4 and graphene coated NCM811	80% for 700 cycles at 0.5C (2.8-4.2 V, NCM811|Gr)	[61]
Physical mixing for 5 min at 2600 rpm	5	$LiFePO_4$ nanoplates coated NCM622	86.5% for 1000 cycles at 1C (2.7-4.55 V, NCM622|Gr)	This work

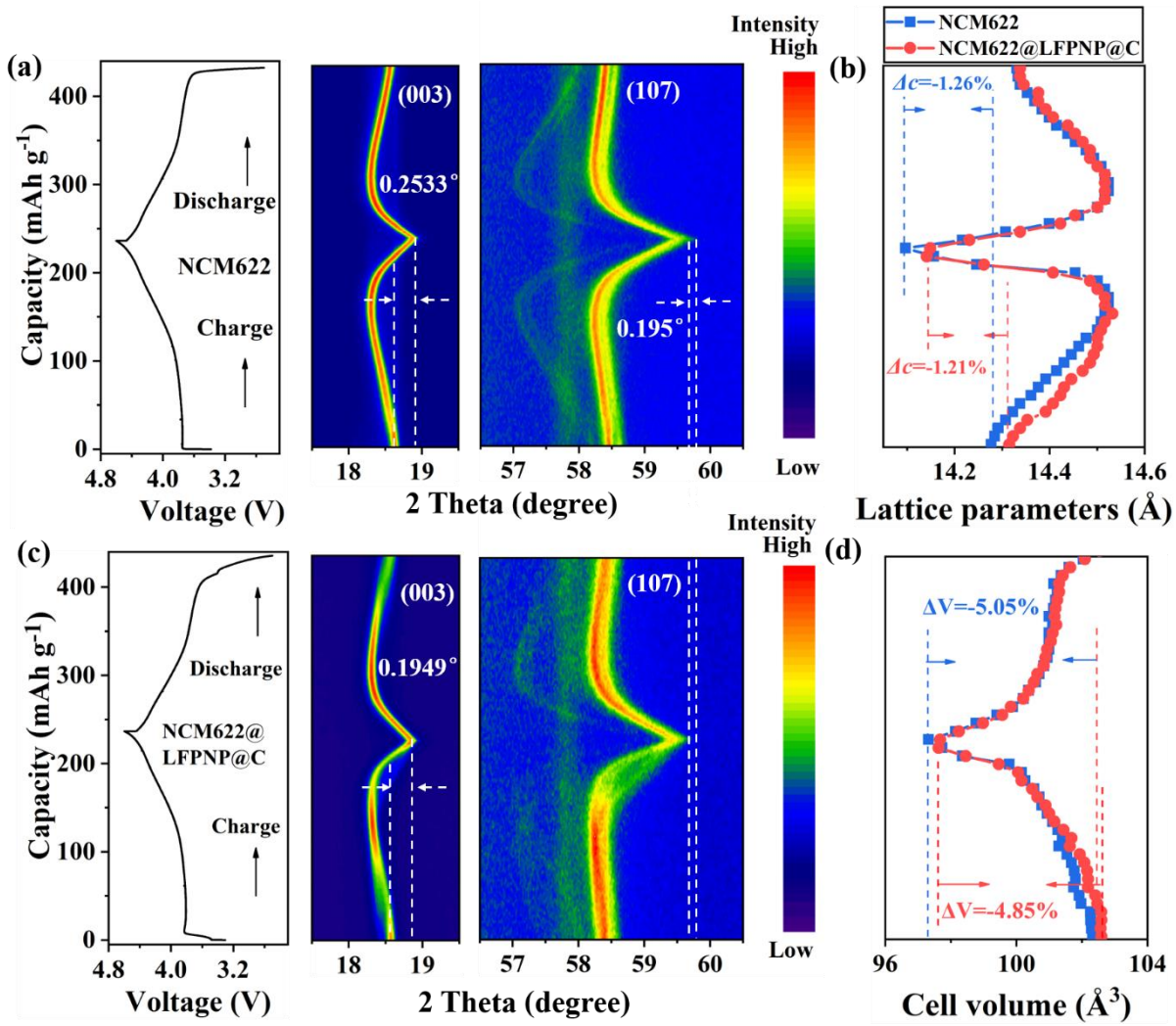

Fig. 3 Evolution of (003) and (107) diffraction peaks of NCM622 (a) and NCM622@LFPNP@C (c) characterized by *in situ* XRD during the first cycle, as well as the variations of *c*-axis lattice parameters (b) and cell volume (d) as a function of the capacity.

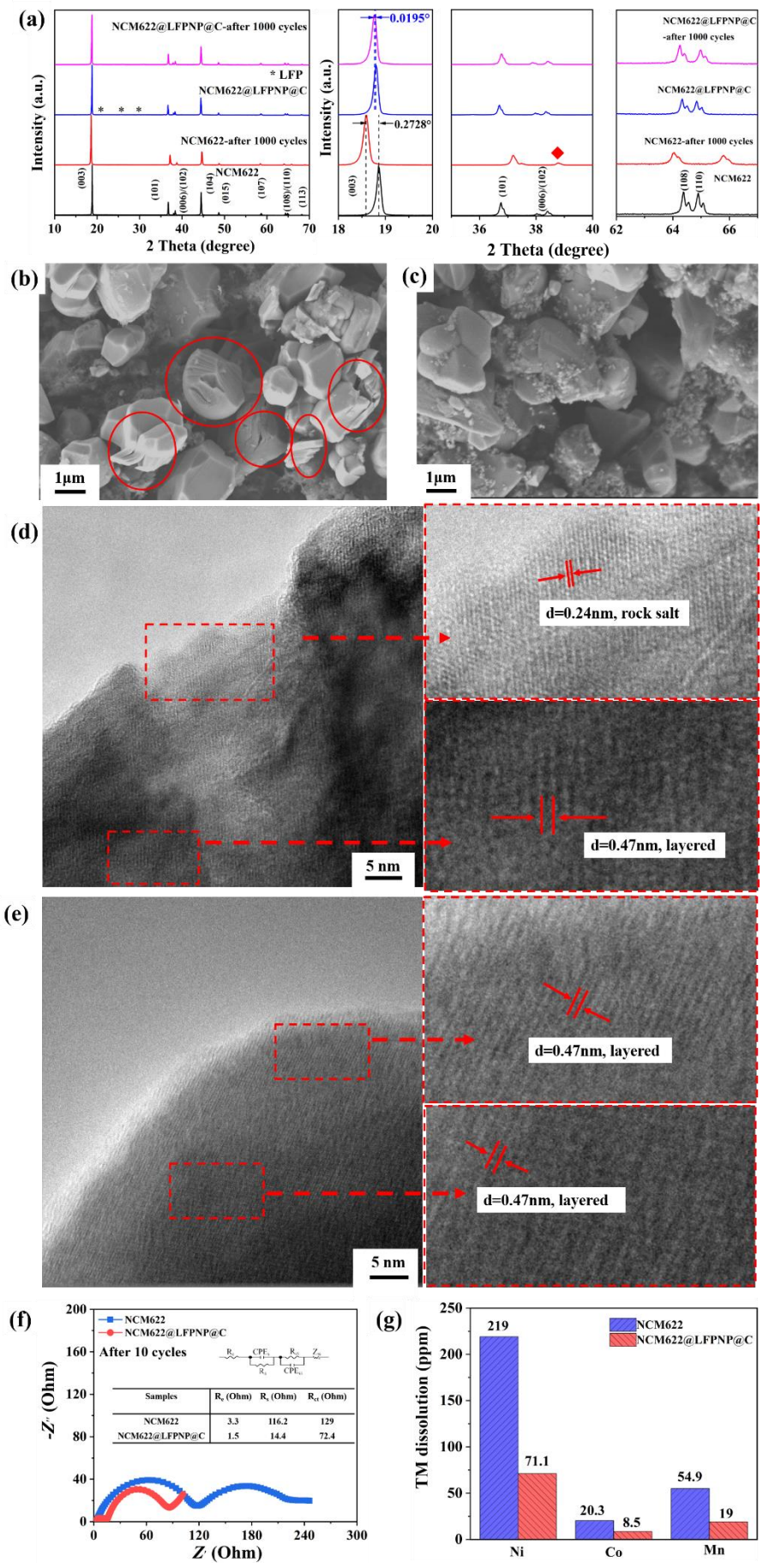
(a)
NCM622@LFPNP@C-after 1000 cycles
* LFP
NCM622@LFPNP@C
NCM622-after 1000 cycles
Intensity (a.u.)
2 Theta (degree)
0.0195°
0.2728°
NCM622
(b)
1μm
(c)
1μm
(d)
d=0.24nm, rock salt
d=0.47nm, layered
5 nm
(e)
d=0.47nm, layered
d=0.47nm, layered
5 nm
(f)
NCM622
NCM622@LFPNP@C
After 10 cycles
Samples
NCM622 3.3 116.2 129
NCM622@LFPNP@C 1.5 14.4 72.4
-Z'' (Ohm)
Z' (Ohm)
(g)
NCM622
NCM622@LFPNP@C
TM dissolution (ppm)
219
71.1
20.3
8.5
54.9
19
Ni
Co
Mn

Fig. 4 The structural characterizations of the NCM622 and NCM622@LFPNP@C cathode after 1000 cycles at 1C in the range of 2.75-4.55 V. XRD (a) and SEM images (b-c) of NCM622 and NCM622@LFPNP@C. HRTEM images of 1000th cycled NCM622 (d) and NCM622@LFPNP@C (e). EIS spectra of NCM622|Li and NCM622@LFPNP@C|Li half cell after 10 cycles with an inset image of the equivalent circuit model (f). The transition metal (TM) elements are detected on the anode after 1000 cycles (g).

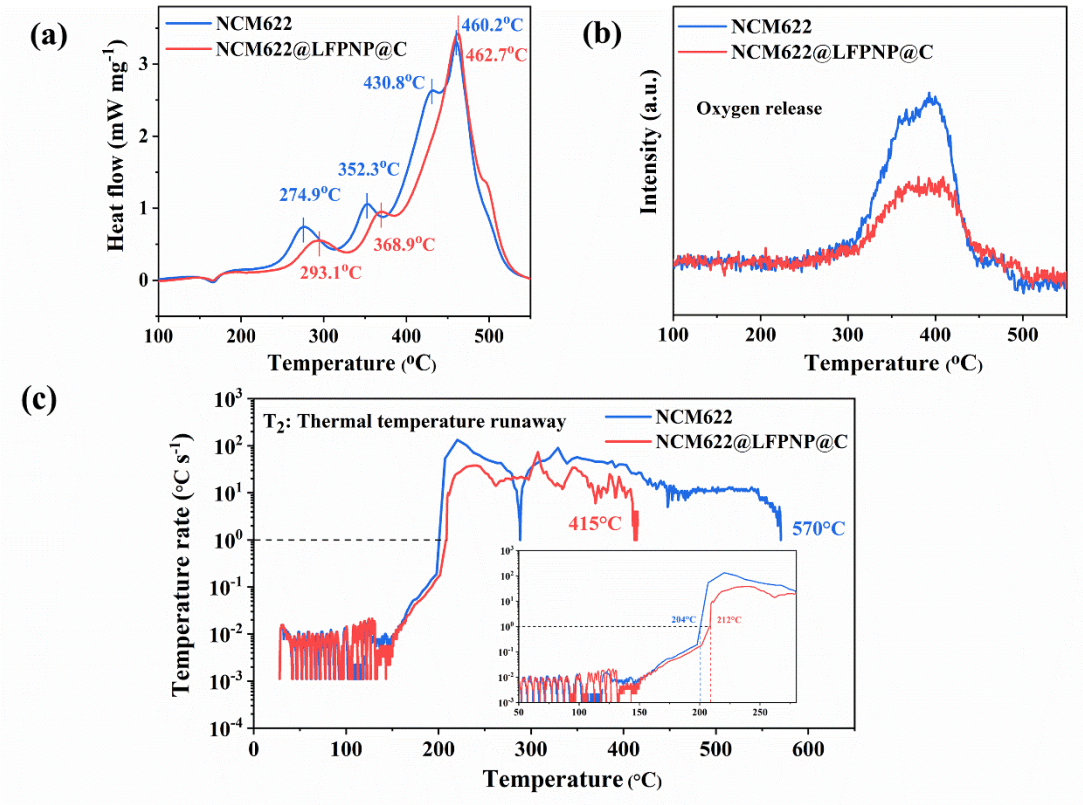

Fig. 5 (a) DSC curves of NCM622 and NCM622@LFPNP@C cathodes, disassembled from half cells charged to 4.3 V. (b) O_2 release of delithiated NCM622 and NCM622@LFPNP@C during heating. (c)Thermal runaway behaviors of 4.5 Ah pouch cells based on NCM622 and NCM622@LFPNP@C cathode materials.

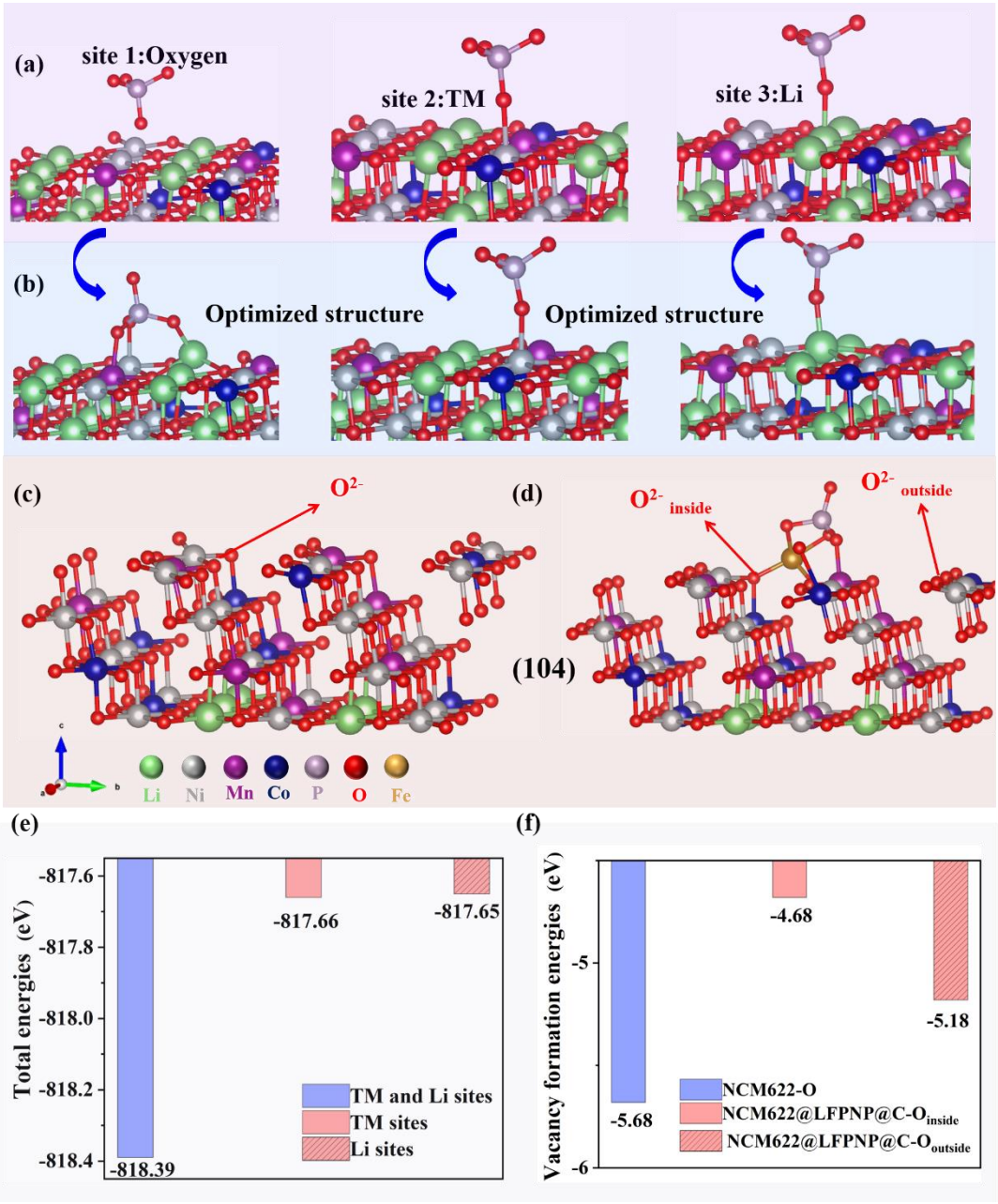

Fig. 6 Three possible sites for PO_4^{3-} adsorption on NCM622(104) surface (a): oxygen sites, transition metal sites, lithium sites. The optimized PO_4^{3-}/NCM622(104) structure (b) and total energy comparisons (e). The initial $Li_{0.13}Ni_{0.6}Co_{0.2}Mn_{0.2}O_2$ (c) and optimized $Li_{0.13}Ni_{0.6}Co_{0.2}Mn_{0.2}O_2/FePO_4$ (d) structures used for O evolution calculations at highly delithiated states: (charge to 4.6V, versus Li/Li^+). The O^{2-} vacancy formation energy of $Li_{0.13}Ni_{0.6}Co_{0.2}Mn_{0.2}O_2$ and $Li_{0.13}Ni_{0.6}Co_{0.2}Mn_{0.2}O_2$/ $FePO_4$ (f).

Biographies and Photographs of the authors

Dr. Qiao Hu is now a postdoctoral researcher in Institute of Nuclear and New Energy Technology (INET), Tsinghua University. She received her B. E. (2015) degree in College of Physical Science and Technology from Central China Normal University and Ph. D. (2020) degree in Material Science from University of Science and Technology of China. Her research focuses on cathode and surface chemistry of lithium-ion batteries.

Dr. Yufang He was born in Hunan, China. She received her bachelor degree in Mechanical Engineering in 2015 from Beijing Technology and Business University, Beijing, P.R. China. In December 2019, she received her Ph.D. degree in Mechanical Engineering from Missouri University of Science and Technology under the supervision of Prof. Jonghyun Park. After her graduation, she dedicated herself to the field of battery research at Tsinghua University, including surface chemistry mechanism of cathode and anode through first-principles and experimental study.

Dr. Dongsheng Ren is now a postdoctoral researcher in Institute of Nuclear and New Energy Technology (INET), Tsinghua University. He received his B. E. (2014) and Ph. D. (2020) degree in School of Vehicle and Mobility, Tsinghua University. His research focuses on electrochemical/thermal modeling of lithium-ion battery.

Dr. Youzhi Song received his Ph.D. degree under Prof. Baoku Zhu from the Department of Polymer Science and Engineering at Zhejiang University in 2018. Currently, he is a postdoctoral in Prof. Xiangming He's group in the Institute of Nuclear and New Energy Technology, Tsinghua University. His current research interests are focused on the rational design of polymeric membrane separators for safe and endurable lithium-based batteries.

Dr. Yanzhou Wu was born in Shandong, China, in 1992. She received her Ph.D. in Institute of Chemistry Chinese Academy of Sciences in 2020. Now, she continues her research in Tsinghua University as a postdoctoral researcher (working with Prof. Xiangming He). Her research is focused on solvation structure of electrolytes of lithium-ion batteries.

Hongmei Liang received her bachelor's and master's degrees from Central South University in 2015 and 2018, respectively. She is currently a PhD candidate with Prof. Xiangming He at the Institute of Nuclear and New Energy Technology, Tsinghua University, China. Her research mainly focuses on lithium metal anode and liquid electrolyte for lithium-ion batteries.

Jinhui Gao was born in Inner Mongolia, China, in 1985. He received his B.S. in Applied Chemistry from Tianjin University in 2008.After graduation, he worked in Tianjin Lishen Battery Joint-Stock Co.,Ltd. In 2020, he started his Eng.D. study under the supervision of Prof. Xiangming He. His research is focused on the failure mechanism for high energy density lithium-ion batteries.

Dr. Gang Xu was born in Liaoning, China, in 1970. He received his Ph.D. from the Institute of Metals Research of the Chinese Academy of Sciences，as a postdoctoral fellow worked in the Department of Physics Chemistry of the Technion-Israel Institute of Technology. He joined Tianjin Lishen Battery Joint-Stock Co., Ltd. in 2021, and served as CTO and president of Lishen Research Institute.

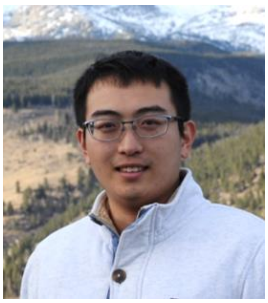

Dr. Jiyu Cai is currently a postdoc research fellow (working with Dr. Zonghai Chen) in Chemical Sciences and Engineering Division at Argonne National Laboratory (Lemont, IL, USA). He received his Ph.D. in Mechanical Engineering (2021) at University of Arkansas. His research is focused on interfacial engineering of advanced electrodes and solid-state electrolytes in lithium-ion batteries.

Dr. Tianyi Li was born in Beijing, China in 1988. He received his B.S. and M.S. in Environmental Engineering from University of Science and Technology Beijing and Oregon State University, respectively. He obtained Ph.D. in Mechanical Engineering from Purdue University West Lafayette. Now, he is a postdoctoral research fellow at Argonne National Laboratory working on solid electrolyte and nickel rich cathode materials in lithium-ion batteries.

Dr. Hong Xu is an associate professor at the Institute of Nuclear and New Energy Technology, Tsinghua University, China. He received his bachelor's degree in polymers at Shanghai Jiao Tong University in 2009 and his PhD in structural molecular science at Institute for Molecular Science in 2015. He is currently an associate professor at Tsinghua University. His research interest lies in the fields of Extreme Ultraviolet Photoresists, Covalent Organic Frameworks, and Lithium-ion Batteries.

Dr. Li Wang is an associate professor at the Institute of Nuclear and New Energy

Technology, Tsinghua University, China. She received his B.S. in 1999 and Ph.D. in Analytical Chemistry in 2004 from the Tsinghua University. Her research expertise includes new electrode material preparation technology, failure mechanism of lithium-ion battery, safety power-battery technology and fundamental understanding of related electrochemical processes.

Dr. Zonghai Chen obtained his PhD from Dalhousie University of Canada (2004), and currently is a chemist at Argonne National Laboratory. His research interest includes functional electrolytes, electrode materials and in situ techniques for advanced lithium-ion batteries. Dr. Chen has authors/co-authored more than 120 peer-reviewed research articles and has a dozen of U.S. patent and patent application.

Dr. Xiangming He is a professor and the group leader of the Lithium-ion battery Laboratory in the Institute of Nuclear and New Energy Technology, Tsinghua University. He received his bachelor's and master's degrees from the School of Chemical Engineering and PhD from Institute of Nuclear and New Energy Technology, Tsinghua University. His research focuses on the design and application of functional materials for energy storage and conversion and fundamental understanding of related electrochemical processes.